Challenges of 9-dB Back-Off Doherty Power Amplifiers with 20% Fractional Bandwidth

Challenges of 9-dB Back-off Doherty Power Amplifiers with 20% Fractional Bandwidth

Zhifan Zhang[1], Anna Piacibello[1], and Vittorio Camarchia[1]

Department of Electronics and Telecommunications, Politecnico di Torino, Italy
{zhifan.zhang, anna.piacibello, vittorio.camarchia}@polito.it.

Abstract. This paper addresses the critical weakness of the conventional Doherty Power Amplifier when targeting wideband and deep back-off operation. A load modulation network with a good trade-off between complexity and performance enhancement is proposed for broadband operation around 9-dB back-off. As an initial assessment, its effectiveness in enhancing the performance in broadband operation has been proven using linear simulations.

Keywords: Deep back-off, Doherty power amplifier, sub-6 GHz.

1 Introduction

With the rapid growth of wireless communication systems, a sharp rise in data traffic poses significant challenges on implementation of radio frequency (RF) power amplifiers (PAs) in wireless transmitters. Among these, the efficiency versus linearity trade-off has become key to the development of the technologies as well as the architectures, especially due to the increasingly high Peak-to-Average Power Ratio (PAPR) and wide instantaneous bandwidth of the adopted modulations [1–4]. Furthermore, in some applications the thermal aspects [5–7] often severely constrain the achievable performance.

The Doherty Power Amplifier (DPA) has become a trendy option in 5G scenario due to its flexible circuit structure, reliable performance and most important property of providing high efficiency at significant output power back-off (OBO) level [8–12] compared to non-load modulated PAs such as class-AB [13–15] and harmonically tuned [16–19] PAs.

However, the conventional DPA struggles to fully meet the requirement outlined in 5G scenario due to its bandwidth limitations and 6-dB OBO efficiency enhancement. This work studies some of the possible topologies of the load modulation network (LMN) for a 9-dB DPA targeting relatively broadband ($\approx 20\%$) operation below 6 GHz.

2 Definition of the simulation setup

In this preliminary study, a set of linear simulations based on the assumed optimum load at the drain current generator plane of the DPA configuration was

used to initially estimate the achievable bandwidth of conventional and proposed LMN. As Fig. 1(a) shows, the output of the Main and Auxiliary amplifiers are initially modelled as ideal current generators synchronously controlled by the respective input voltages.

In a 9-dB OBO DPA configuration, the Auxiliary generator is initially off, until the Main amplifier current I_{M} reaches $\gamma\, I_{\mathrm{M,max}}$, where $I_{\mathrm{M,max}}$ is the maximum Main drain current and $\gamma = 1/3$. This refers to a 9.6-dB input back-off power level, which is typically compatible with an OBO level around 9 dB due to the unavoidable gain compression at saturation in GaN PAs. Moreover, under the assumption that both devices operate at the same drain voltage supply, the ratio of the Auxiliary and Main active peripheries scales like the ratio of the maximum drain currents: $\beta = I_{\mathrm{A}}/I_{\mathrm{M}} = 2$.

The drain current profiles I_{M} and I_{A} of the Main and Auxiliary amplifiers are expressed by (1), (2) [20] and plotted in Fig. 1(b).

$$I_{\mathrm{M}} = x\, I_{\mathrm{M,max}}, \qquad \text{for} \quad 0 \le x \le 1. \tag{1}$$

$$I_{\mathrm{A}} = \begin{cases} 0 & \text{for} \quad 0 \le x < \gamma \\ I_{\mathrm{M,max}} \cdot \beta \cdot \frac{x-\gamma}{1-\gamma}, & \text{for} \quad \gamma \le x \le 1. \end{cases} \tag{2}$$

$$\text{where} \qquad x = \frac{v_{\mathrm{in}}}{v_{\mathrm{in,max}}} = \sqrt{\frac{\mathrm{P_{in}}}{\mathrm{P_{in,max}}}}. \tag{3}$$

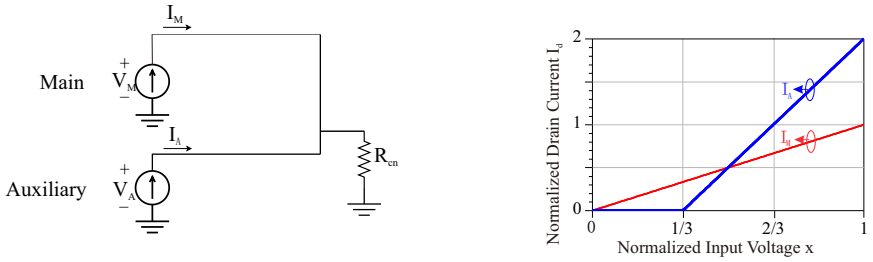

(a) (b)

Fig. 1: (a) DPA configuration and (b) drain current profiles of the Main and Auxiliary amplifier in 9-dB OBO DPAs.

3 Preliminary Study of LMN in a GaN 9-dB OBO DPA

Considering the parameters of a typical GaN technology [21] suited for application up to X band, i.e., $V_{\mathrm{DD}} = 28\,\mathrm{V}$ and a power density of $4\,\mathrm{W/mm}$, for a

design aimed at delivering around 75 W of saturated power, the resulting optimum loads are $R_{\mathrm{opt,M}} = 16\,\Omega$ and $R_{\mathrm{opt,A}} = 8\,\Omega$ assuming the same supply voltage is adopted for both. The LMN is required to present $3\,R_{\mathrm{opt,M}}$ to the Main amplifier at the 9-dB OBO power level, $R_{\mathrm{opt,M}}$ and $R_{\mathrm{opt,A}}$ to the current plane of the Main and the Auxiliary ones at saturation.

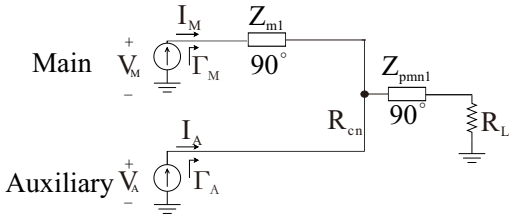

(a)

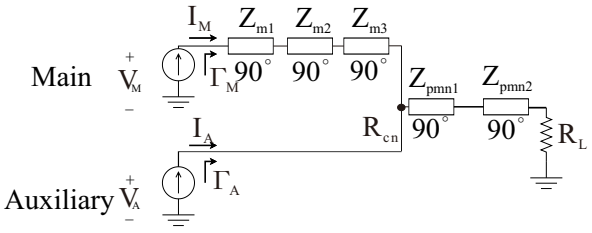

(b)

Fig. 2: Block diagrams of (a) conventional and (b) proposed DPA.

A conventional DPA architecture, made of two quarter-wavelength transmission lines (QWTs) with characteristic impedance Z_{m1} and Z_{pmn1} acting as inverter and post-matching, is shown in Fig. 2(a). Typically, the single QWT tends to narrow the bandwidth over which the optimal load modulation occurs. Thus, an alternative broadband LMN, shown in Fig. 2(b), is proposed to improve the DPA performance. The common node is connected through a three-section QWT-constructed impedance inverter to the Main, and a two-section QWT PMN is adopted to match the common node load R_{cn} to $50\,\Omega$. This topology has additional degrees of freedom, which allows optimizing the loads at OBO and at saturation with different trade-offs.

3.1 Static transistor model

Assuming that the parasitic effects of the devices are negligible, or can be ideally cancelled over the target band, the ideal current generators can fully model the devices' outputs to initially evaluate the effectiveness of the modified LMN.

The conventional and proposed LMNs are implemented with the circuit parameters provided in Table 1, and the corresponding results are illustrated in Fig. 3. The circuit parameters for the conventional combiner can either be obtained analytically by solving the equations reported in (4) at center frequency, or optimized numerically to trade-off the matching condition at OBO and saturation, thus allowing to cover a wider bandwidth.

It is worth mentioning that the resulting characteristic impedances are rather low in all cases, but are especially critical for the proposed LMN. This may hinder its implementation is some specific technology, and in any case calls for careful layout planning and electromagnetic simulation of the passive networks as well as the transition between them and the terminals of the transistors. In case the resulting impedance levels were too low, the options are either to constrain them by accepting a worse bandwidth matching trade-off or to consider lumped implementation of the QWTs. These considerations are however difficult to treat in a general analysis due to the high number of variants.

Table 1: Circuit parameters for the combiners of Fig. 2

Circuit		Z_{m1}	Z_{m2}	Z_{m3}	Z_{pmn1}	Z_{pmn2}	Unit
Fig. 2(a)	analytical	16	-	-	16	-	Ω
	optimized	23	-	-	20	-	Ω
Fig. 2(b)	optimized	27	9	6	12	34	Ω

$$R_{\mathrm{opt,M}} = \frac{{Z_{\mathrm{m1}}}^2}{R_{\mathrm{cn}}}; R_{\mathrm{cn}} = \frac{{Z_{\mathrm{pmn1}}}^2}{R_{\mathrm{L}}}. \tag{4}$$

Fig. 3(a) compares the performance that can be obtained by the conventional LMN, in terms of load synthesized at the current generator planes and corresponding efficiency. The dashed lines refer to the analytical solution exact at f_0, whereas the solid lines to the numerically optimized one.

In both cases, the load modulation line at f_0 is well located at the real axis in the Smith chart with the synthesized loads at OBO and saturation, reaching the optimum value. Conversely, at frequencies that deviate from f_0, ranging from $0.9\,f_0$ to $1.1\,f_0$, the load modulation trajectories are symmetrically distributed across the inductive and capacitive region along the centered real axis. The Auxiliary load at saturation and the Main load at OBO remain approximately close to the optimum impedance, despite the load at saturation of the Main deviates significantly from the optimal load target as the frequency shifts from f_0.

At the critical power level, the Auxiliary load maintains a relatively stable matching over a 20% fractional bandwidth, while the Main load at OBO remains below -10 dB across a 15% bandwidth but deteriorates when it comes to a 20% one. Even if the loading condition at saturation is less constant and remains

below -10 dB only in a 10% fractional bandwidth, the efficiency in this ideal case can be still optimized to remain over 60% at both OBO and saturation over a 20% fractional bandwidth. In this first evaluation the bandwidth is estimated by an approximate method that does not account for voltage clipping.

Fig. 3(b) illustrates how the proposed LMN is capable to synthesize the net-like load modulation curves, offering the potential to achieve a trade-off for optimal matching at either OBO or saturation of the Main over the bandwidth. The simulation results demonstrate that the proposed LMN achieves a trade-off for improved matching at Main saturation across the bandwidth, while maintaining good matching for other loading condition with a margin over a 20% fractional bandwidth. Consequently, it shows a 75% saturation efficiency over the band, meanwhile still maintaining over 60% OBO efficiency. Compared to conventional LMNs, this topology improves the overall performance and offers greater flexibility in achieving design objectives. This enables the DPA to operate efficiently in the 9-dB OBO and saturation regions.

3.2 Effect of transistors' parasitics

In practice, parasitic effects are hardly ever completely negligible in current applications and should therefore be taken into consideration.

Since the proposed analysis should hold for a typical GaN/SiC technology, the parasitic parameters of the Main and Auxiliary amplifiers are assumed to be modelled by a shunt-C and series-L network with values per unit gate width of 0.35 pF/mm and 3 pH/mm, respectively, which are assumed to scale linearly with the device periphery W.

For a design focusing on achieving 75 W saturated power, the scaled parasitic capacitance are estimated as $C_{\mathrm{out,M}} = 2\,\mathrm{pF}$, $L_{\mathrm{out,M}} = 15\,\mathrm{pH}$ and $C_{\mathrm{out,A}} = 4\,\mathrm{pF}$, $L_{\mathrm{out,M}} = 30\,\mathrm{pH}$ [22]. In this case, a simple L-section network cascaded at the output of the Main and Auxiliary amplifiers, as presented in Fig. 4, is introduced to compensate for the parasitic effects over target band [23].

Consequently, the conventional and proposed LMNs topologies incorporate an additional compensation network illustrated in Fig.4 to synthesize the desired load modulation across the bandwidth. The characteristic impedance of each transmission line is re-optimized numerically together with the circuit parameters of the parasitic compensation networks, to achieve the best matching conditions for both Main and Auxiliary simultaneously over a 20% fractional bandwidth. The resulting circuit parameters are summarized in in Table 2 and in Table 3.

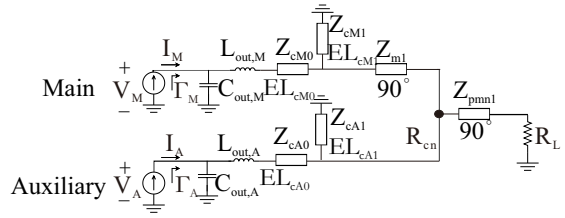

(a)

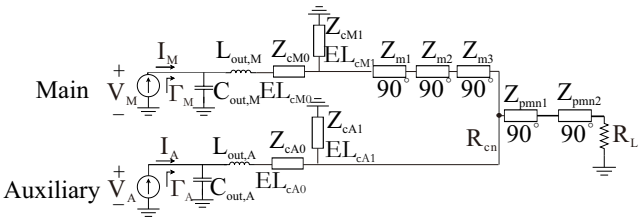

(b)

Fig. 4: Block diagrams of (a) conventional and (b) proposed DPA incorporating with a L-section compensator.

Table 2: Circuit parameters for the parasitic compensation networks of Fig. 4

Circuit	Z, θ_{cM0}	Z, θ_{cM1}	Z, θ_{cA0}	Z, θ_{cA1}	Unit
Fig. 4(a)	58, 8	48, 18	5, 1	82, 6	Ω, °
Fig. 4(b)	79, 1	90, 13	20, 1	90, 7	Ω, °

Table 3: Circuit parameters for the combiners of Fig. 4

Circuit	Z_{m1}	Z_{m2}	Z_{m3}	Z_{pmn1}	Z_{pmn2}	Unit
Fig. 4(a)	19	-	-	24	-	Ω
Fig. 4(b)	31	13	6	10	35	Ω

The performance of the modified LMNs are depicted in in Fig. 5. For the re-optimized conventional LMN, the Main matching condition at saturation improved to -15 dB across a 15% fractional bandwidth. However, it degrades the matching condition of Main at OBO and Auxiliary at saturation respectively. As a result, the saturation efficiency deteriorates over band.

Conversely, the proposed LMN after optimization is able to maintain -15 dB matching referring to all the desired load across a 20% fractional bandwidth. Moreover, the matching at the center frequency improved towards -30 dB with the assistance of the compensation network. As a consequence, it leads to the performance enhancement over band. Overall, the performance considering the impact of parasitic effects closely aligns with the ideal case, demonstrating the effectiveness of the proposed LMN.

4 Conclusion

This paper has discussed some of the challenges existing in the implementation of wideband DPAs for deep OBO operation, such as the presence of transistor parasitic effects to be compensated (which strongly depends on technology) and the feasibility of the QWT dimensions, and has proposed a load modulation network to enhance the bandwidth of a Doherty PA for 9-dB OBO. In fact, the targeted loads lead to rather low values for $Z_{\mathrm{m2,3}}$, which pose a challenge for the DPA layout. Consequently, a MMIC implementation is impractical due to the wide transmission lines required, not prone to bending and fitting a compact layout. Conversely, a PCB implementation of the combiner which avoids bends is feasible. If packaged transistors are adopted, the achievable bandwidth has to be reconsidered including the parasitic effects caused by the packaging. A promising alternative for sub-6-GHz operation is a PCB-based design using bare dies, which only needs to embed the effect of short bondwires in the combiner QWTs.

References

1. A. Piacibello et al., "High-Gain and High-Linearity MMIC GaN Doherty Power Amplifier With 3-GHz Bandwidth for Ka-Band Satellite Communications," in IEEE Microwave and Wireless Technology Letters, **34**(6), 765-768(2024)
2. R. Giofrè et. al. "A Design Approach to Maximize the Efficiency vs. Linearity Trade-Off in Fixed and Modulated Load GaN Power Amplifiers," in IEEE Access, vol. 6, pp. 9247-9255(2018)
3. S. Zhao, et. al. "Linearity Improved Doherty Power Amplifier Using Non-Foster Circuits," in IEEE Access, vol. 7, pp. 40109-40113(2019)
4. R. Sharma Nitesh, et. al. "A 700MHz to 2.5GHz Cascode GaAs Power Amplifier for Multi-Band Pico-Cell Achieving 20dB Gain, 40dBm to 45dBm OIP3 and 66% Peak PAE," in IEEE Access, vol. 6, pp. 818-829(2018)
5. Y. Wang and R. Naylor, "Challenges in designing 5 GHz 802.11ac WiFi power amplifiers," 2014 IEEE Topical Conference on Power Amplifiers for Wireless and Radio Applications , Newport Beach, CA, USA, 2014, pp. 16-18
6. C. Ramella et al., "Thermal-aware GaN/Si MMIC design for space applications," 2019 IEEE International Conference on Microwaves, Antennas, Communications and Electronic Systems (COMCAS), Tel-Aviv, Israel, 2019, pp. 1-6.
7. F. Costanzo et al., "A Derating-Rules Compliant Ka-Band GaN-on-Si Power Amplifier Designed for Highly Reliable Satellite Applications," 2021 16th European

Microwave Integrated Circuits Conference, London, United Kingdom, 2022, pp. 253-256
8. G. Nikandish, et. al, "Breaking the Bandwidth Limit: A Review of Broadband Doherty Power Amplifier Design for 5G," IEEE Microw. Mag. **21**(4), 57–75, (2020).
9. X.-H. Fang, et. al. "Modified Doherty amplifier with extended bandwidth and back-off power range using optimized peak combining current ratio," IEEE Trans. Microw. Theory Techn. **66**(12), 5347–5357 (2018)
10. S. Chen, et. al. "A bandwidth enhanced Doherty power amplifier with a compact output combiner," IEEE Microw. Wireless Compon. Lett. **26**(6), 434–436 (2016)
11. A. Piacibello, et. al. "3-Way Doherty Power Amplifiers: Design Guidelines and MMIC Implementation at 28 GHz," IEEE Trans. Microw. Theory Techn. **71**(5), 2016–2028 (2022).
12. A. Pitt, et. al. "A Broadband Asymmetrical Doherty Power Amplifier With Optimized Continuous Mode Harmonic Impedances," IEEE J. of Microw. **3**(4), 1120–1133 (2023)
13. M. Iqbal and A. Piacibello, "A 5W class-AB power amplifier based on a GaN HEMT for LTE communication band," 2016 16th Mediterranean Microwave Symposium (MMS), Abu Dhabi, United Arab Emirates, 2016, pp. 1-4.
14. A. S. M. Alqadami, et. al. "A 5 W high efficiency Class AB power amplifier for LTE base station application," 2017 28th Irish Signals and Systems Conference, Killarney, Ireland, 2017, pp. 1-5
15. A. Gadallah, et. al. "A high efficiency 3–7 GHz class AB CMOS power amplifier for WBAN applications," 2015 IEEE International Symposium on Radio-Frequency Integration Technology, Sendai, Japan, 2015, pp. 163-16
16. A. Piacibello, Z. Zhang and V. Camarchia, "Continuous Inverse Class-F GaN Power Amplifier with 70% Efficiency over 1.4-2 GHz Bandwidth," 2023 IEEE Topical Conference on RF/Microwave Power Amplifiers for Radio and Wireless Applications, Las Vegas, NV, USA, 2023, pp. 10-12.
17. Y. -W. Duan, et. al. "Low-Voltage Continuous Class-F Wideband Power Amplifier," in IEEE Microwave and Wireless Technology Letters, **34**(6), 639-642 (2024)
18. T. Sharma, et.al. "Generalized Continuous Class-F Harmonic Tuned Power Amplifiers," in IEEE Microwave and Wireless Components Letters, **26**(3), 213-215 (2016)
19. C. Chu, et.al. "High-Efficiency Class-iF-1 Power Amplifier With Enhanced Linearity," in IEEE Transactions on Microwave Theory and Techniques, **71**(5), 1977-1989(2023)
20. G. Ghione and M. Pirola. "Microwave Electronics". UK, Cambridge University Press, 2018 Forum (2002)
21. V. Camarchia, et. al. "Fabrication and nonlinear characterization of GaN HEMTs on SiC and sapphire for high-power applications," Int J RF and Microwave Comp Aid Eng, 16: 70-80, (2006).
22. A. Stillmaker, et. al. "Scaling equations for the accurate prediction of CMOS device performance from 180nm to 7nm," IEEE Trans. Microw. Theory Techn. 58, 74-81 (2017)
23. J. M. Rubio, et. al. "Design of an 87% Fractional Bandwidth Doherty Power Amplifier Supported by a Simplified Bandwidth Estimation Method," IEEE Trans. Microw. Theory Techn. **66**(3), 1319-1327 (2018)

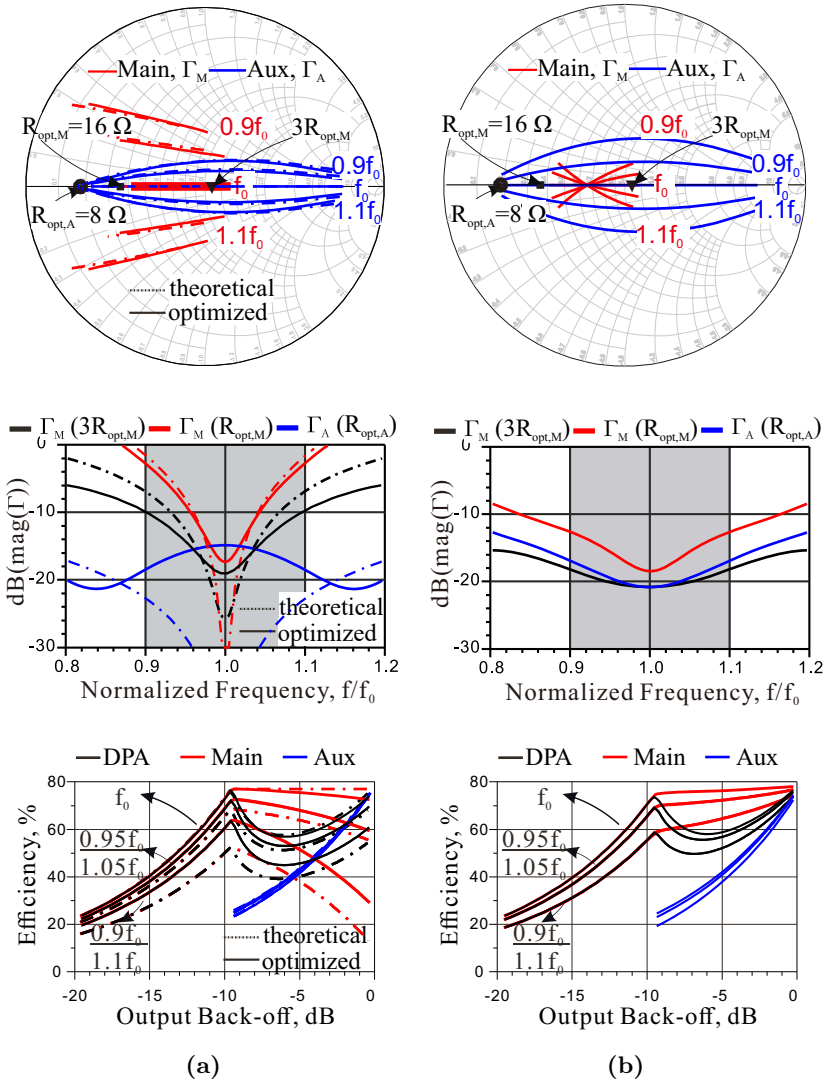

Fig. 3: Performance of the combiners of Fig. 2(a) and Fig. 2(b), in terms of synthesized loads and corresponding efficiency.

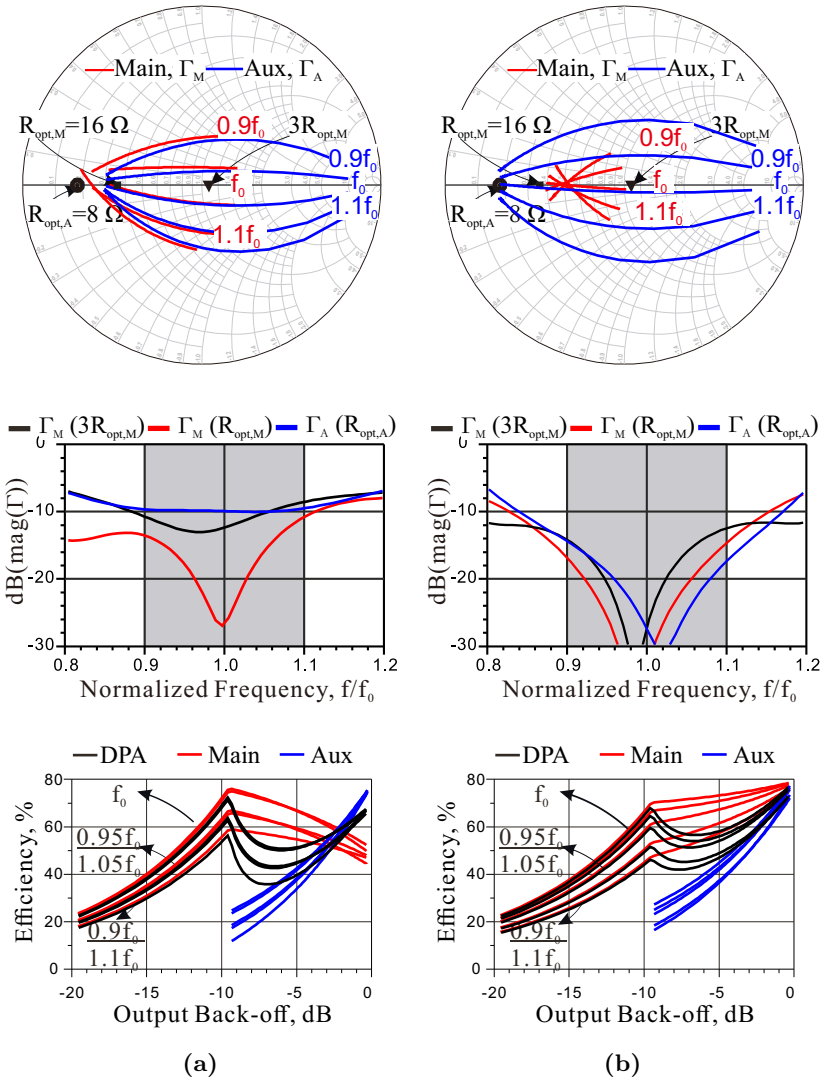

Fig. 5: Performance of the combiners of Fig. 4(a) and Fig. 4(b), in terms of synthesized load and corresponding efficiency.